

SPLITTING SCHEMES FOR A NAVIER-STOKES-CAHN-HILLIARD MODEL FOR TWO FLUIDS WITH DIFFERENT DENSITIES*

Francisco Guillén-González

*Departamento de Ecuaciones Diferenciales y Análisis Numérico and IMUS, Universidad de Sevilla,
41012 Seville, Spain
Email: guillen@us.es*

Giordano Tierra

*Department of Applied and Computational Mathematics and Statistics, University of Notre Dame,
Notre Dame, IN 46556, USA
Email: gchica@nd.edu*

*Current address: Mathematical Institute, Faculty of Mathematics and Physics, Charles University,
Prague 8, 186 75, Czech Republic
Email: gtierra@karlin.mff.cuni.cz*

Abstract

In this work, we focus on designing efficient numerical schemes to approximate a thermodynamically consistent Navier-Stokes/Cahn-Hilliard problem given in [3] modeling the mixture of two incompressible fluids with different densities. The model is based on a diffuse-interface phase-field approach that is able to describe topological transitions like droplet coalescence or droplet break-up in a natural way. We present a splitting scheme, decoupling computations of the Navier-Stokes part from the Cahn-Hilliard one, which is unconditionally energy-stable up to the choice of the potential approximation. Some numerical experiments are carried out to validate the correctness and the accuracy of the scheme, and to study the sensitivity of the scheme with respect to different physical parameters.

Mathematics subject classification: 35Q35, 65M60, 76D05, 76D45, 76T10.

Key words: Two-phase flow, Diffuse-interface phase-field, Cahn-Hilliard, Navier-Stokes, Energy stability, Variable density, Mixed finite element, Splitting scheme.

1. Introduction

The evolution in time of the interface of two or more immiscible fluids arise naturally in hydrodynamics and materials science for modeling many current scientific, engineering, and industrial applications.

In recent times, the diffuse-interface approach has been used to describe the dynamic of the interfaces by layers of small thickness. One fundamental advantage of these models is that they are able to describe topological transitions like droplet coalescence or droplet break-up in a natural way.

The diffuse-interface theory was originally developed as methodology for modeling and approximating solid-liquid phase transitions. This idea can be traced to van der Waals [25], and is the foundation for the phase-field theory for phase transition and critical phenomena. Thus,

* Received July 12, 2013 / Revised version received April 3, 2014 / Accepted May 26, 2014 /
Published online September 3, 2014 /

the structure of the interface is determined by molecular forces; the tendencies for mixing and de-mixing are balanced through a non-local mixing energy.

Hohenberg and Halperin presented in [19] the so-called *Model H*, in order to model two incompressible, viscous Newtonian fluids with the same density. In [18], Gurtin et al. arrived at the same model by using the rational continuum mechanics framework and showed that it satisfies the second law of thermodynamics, leading in both cases to the so-called Navier-Stokes/Cahn-Hilliard system (NSCH).

There are many works devoted to study numerical schemes to approximate NSCH model that in the most of cases consists on coupling schemes previously presented for Navier-Stokes (see for instance [12]) and Cahn-Hilliard system [8–10]. In [22], the author study numerically a NSCH model (for the case of three phases) presenting a splitting and unconditionally stable scheme (satisfying a discrete energy law).

In the last years, many authors have been concerned in designing models to describe the flow of two incompressible, viscous Newtonian fluids with different densities. Lowengrub and Truskinovsky derived in [21] a thermodynamically consistent extension of the NSCH model with different densities but in this case the velocity field is no longer divergence free, leading to new difficulties to design fully discrete numerical schemes. Recently, Abels has discussed in [1] about the existence of local in time strong solutions of the system derived in [21]. A new related approach has been presented in [24] where mass and volume conservation is obtained for binary fluids and some splitting numerical schemes are proposed, although no discrete energy laws satisfied by the schemes are provided.

In [4], Boyer gives the complete derivation and a numerical approach of a model for the study of incompressible two-fluids mixture with different densities and viscosities, although no energy law of the system is presented.

There is also an increasing interest in more general models that are able to capture the mixture of different complex fluids. We refer the reader to [26] for a general formulation using the diffuse-interface method, to [7] for energy stable schemes for the Cahn-Hilliard-Brinkman equation and to [6] for energy stable schemes for anisotropic Cahn-Hilliard systems.

On the other hand, Shen and Yang presented in [23] a model and numerical approximations for two-phase incompressible flows with different densities and viscosities. In [27], Zhang and Wang present a study of the influence of the mobility term in a model of two-phase incompressible flows with different densities but no physical background of the derivation of the model is presented or cited. Finally, Abels et al. derived in [3] a new thermodynamically consistent model for incompressible two-phase flows with different densities while in [2] the existence of weak solutions for this model is proved. For a recent review in multi-component mixtures using phase field models we refer the reader to [20].

In this work, we present an unconditionally energy-stable and splitting scheme to approximate the model derived by Abels et al. in [3], showing its validity by several numerical simulations. In fact, the scheme decouples computations of the Navier-Stokes part from the Cahn-Hilliard one, and it is unconditionally energy-stable up to the choice of the potential approximation.

The rest of the paper is organized as follows. In Section 2, we detail the model considered and its energy law. The splitting numerical scheme and its energy-stability are derived in Section 3. In Section 4 we present some 2D and 3D numerical simulations and we state some conclusions in Section 5. Finally, the well-posedness of the scheme is proved in an Appendix.

2. The Model

Let $\Omega \subset \mathbb{R}^d$ ($d = 2, 3$) be a bounded domain, occupied by a mixture of two immiscible and incompressible fluids with different (and constant) densities $\rho_1 > \rho_2 > 0$. We denote $Q = \Omega \times (0, +\infty)$.

Considering there is a mixing interface (of small thickness), the following NSCH model satisfied in Q has been introduced by Abels et al. [3]:

$$\left\{ \begin{array}{l} \rho \mathbf{u}_t + \left((\rho \mathbf{u} + \mathbf{J}) \cdot \nabla \right) \mathbf{u} - \nabla \cdot (2\eta(\phi) \mathbf{D}\mathbf{u}) + \nabla p + \lambda \varepsilon \nabla \cdot (\nabla \phi \otimes \nabla \phi) = 0, \\ \nabla \cdot \mathbf{u} = 0, \\ \rho_t + \nabla \cdot (\rho \mathbf{u} + \mathbf{J}) = 0, \\ \phi_t + \mathbf{u} \cdot \nabla \phi - \nabla \cdot (m(\phi) \nabla w) = 0, \\ -\lambda \varepsilon \Delta \phi + \frac{\lambda}{\varepsilon} f(\phi) = w. \end{array} \right. \quad (2.1)$$

Here \mathbf{u} represents the mean velocity, p the pressure and ρ the density of the mixture, while ϕ is an order parameter (related to the difference of the volume fraction of each fluid) and w is the so-called chemical potential. Moreover, $\eta(\phi) > 0$ is the viscosity of the mixture (depending on the phase), λ is a constant related to the surface energy density, $\varepsilon > 0$ is a (small) parameter related to the thickness of the interface between the two fluids and $\mathbf{D}\mathbf{u} = \frac{1}{2}(\nabla \mathbf{u} + \nabla \mathbf{u}^t)$. From now on, we are going to consider the Ginzburg-Landau double well potential

$$F(\phi) = \frac{1}{4}(\phi^2 - 1)^2$$

with minima in ± 1 (representing the pure phases) and

$$f(\phi) = F'(\phi) = (\phi^2 - 1)\phi.$$

Moreover, $m(\phi) > 0$ is the mobility function and

$$\mathbf{J} = -\frac{\rho_1 - \rho_2}{2} m(\phi) \nabla w$$

is a relative mass flux related to the diffusion of the components. Since $\rho_1 - \rho_2 > 0$, this relative flux moves from high to low concentration of the chemical potential w . This relative flux \mathbf{J} vanishes in the case of matched densities $\rho = \rho_2 = \rho_1 = \text{const}$.

Note that, taking into account ϕ -equation (2.1)₄, then ρ -equation (2.1)₃ is equivalent to the explicit relation

$$\rho(\phi) = \frac{\rho_1 + \rho_2}{2} + \frac{\rho_1 - \rho_2}{2} \phi := \rho_{med} + \rho_{dif} \phi. \quad (2.2)$$

Indeed, from (2.2) $\rho'(\phi) = \rho_{dif}$ (a positive constant) and

$$\mathbf{J} = -\rho_{dif} m(\phi) \nabla w = -\rho'(\phi) m(\phi) \nabla w,$$

hence

$$\rho_t + \nabla \cdot (\rho \mathbf{u} + \mathbf{J}) = \rho'(\phi) \left(\phi_t + \mathbf{u} \cdot \nabla \phi - \nabla \cdot (m(\phi) \nabla w) \right) = 0.$$

On the other hand, since

$$\begin{aligned} \lambda\varepsilon\nabla \cdot (\nabla\phi \otimes \nabla\phi) &= \lambda\varepsilon\Delta\phi\nabla\phi + \frac{\lambda\varepsilon}{2}\nabla(|\nabla\phi|^2) \\ &= \left(\lambda\varepsilon\Delta\phi - \frac{\lambda}{\varepsilon}f(\phi)\right)\nabla\phi + \nabla\left(\frac{\lambda\varepsilon}{2}|\nabla\phi|^2 + \frac{\lambda}{\varepsilon}F(\phi)\right), \end{aligned}$$

we can rewrite the problem (2.1) as follows:

$$\left\{ \begin{array}{l} \rho(\phi)\mathbf{u}_t + \left((\rho(\phi)\mathbf{u} - \rho_{dif}m(\phi)\nabla w) \cdot \nabla\right)\mathbf{u} - \nabla \cdot (2\eta(\phi)\mathbf{D}\mathbf{u}) + \nabla\tilde{p} - w\nabla\phi = 0, \\ \nabla \cdot \mathbf{u} = 0, \\ \phi_t + \mathbf{u} \cdot \nabla\phi - \nabla \cdot (m(\phi)\nabla w) = 0, \\ -\lambda\varepsilon\Delta\phi + \frac{\lambda}{\varepsilon}f(\phi) = w. \end{array} \right. \tag{2.3}$$

where the density $\rho(\phi)$ is computed from (2.2) and the following modified potential appears:

$$\tilde{p} = p + \frac{\lambda\varepsilon}{2}|\nabla\phi|^2 + \frac{\lambda}{\varepsilon}F(\phi).$$

For simplicity of notation we write in the following p instead of \tilde{p} .

The PDE system (2.3) is supplemented with the following initial and boundary conditions:

$$\begin{aligned} \mathbf{u}|_{t=0} &= \mathbf{u}_0, \quad \phi|_{t=0} = \phi_0 \quad \text{in } \Omega, \\ \mathbf{u}|_{\partial\Omega} &= 0, \quad \frac{\partial\phi}{\partial n}\Big|_{\partial\Omega} = 0, \quad \frac{\partial w}{\partial n}\Big|_{\partial\Omega} = 0 \quad \text{in } (0, T). \end{aligned}$$

Then, the mixed weak formulation of problem (2.3) can be defined as follows (see the energy law (2.8) below): find (u, p, ϕ, w) such that

$$\begin{aligned} \mathbf{u} &\in L^\infty(0, T; \mathbf{L}^2(\Omega)) \cap L^2(0, T; \mathbf{H}_0^1(\Omega)), \\ \phi &\in L^\infty(0, T; H^1(\Omega)), \quad w \in L^2(0, T; H^1(\Omega)), \end{aligned} \tag{2.4}$$

and, jointly to $\rho(\phi)$ given by (2.2), satisfying the following variational equations,

$$\left\{ \begin{array}{l} \left\langle \rho(\phi)\mathbf{u}_t, \bar{\mathbf{u}} \right\rangle + \left([(\rho(\phi)\mathbf{u} - \rho_{dif}m(\phi)\nabla w) \cdot \nabla]\mathbf{u}, \bar{\mathbf{u}} \right) \\ \quad + 2\left(\eta(\phi)\mathbf{D}\mathbf{u}, \mathbf{D}\bar{\mathbf{u}}\right) - \left(p, \nabla \cdot \bar{\mathbf{u}}\right) - \left(w\nabla\phi, \bar{\mathbf{u}}\right) = 0, \\ \left(\nabla \cdot \mathbf{u}, \bar{p}\right) = 0, \\ \left\langle \phi_t, \bar{w} \right\rangle + \left(\mathbf{u} \cdot \nabla\phi, \bar{w}\right) + \left(m(\phi)\nabla w, \nabla\bar{w}\right) = 0, \\ \lambda\varepsilon\left(\nabla\phi, \nabla\bar{\phi}\right) + \frac{\lambda}{\varepsilon}\left(f(\phi), \bar{\phi}\right) - \left(w, \bar{\phi}\right) = 0, \end{array} \right. \tag{2.5}$$

for each $(\bar{\mathbf{u}}, \bar{p}, \bar{w}, \bar{\phi}) \in \mathbf{H}_0^1(\Omega) \times L_0^2(\Omega) \times H^1(\Omega) \times H^1(\Omega)$. Hereafter, we denote the inner-product in $L^2(\Omega)$ by (\cdot, \cdot) .

Note that, owing to regularity (2.4), this variational formulation has sense, in particular for the time derivative terms in a dual space.

Taking into account the following relations

$$\begin{cases} (w\nabla\phi, \bar{\mathbf{u}}) = (\nabla(\phi w), \bar{\mathbf{u}}) - (\phi\nabla w, \bar{\mathbf{u}}), \\ (\mathbf{u} \cdot \nabla\phi, \bar{w}) = (\nabla \cdot (\phi \mathbf{u}), \bar{w}) = -(\phi \mathbf{u}, \nabla\bar{w}) \end{cases}$$

(in the second relation the incompressibility constraint $\nabla \cdot \mathbf{u} = 0$ has been used) and redefining again the pressure term as

$$\tilde{p} = p - \phi w,$$

we can rewrite (2.5) as (again we write p instead of \tilde{p}):

$$\left\{ \begin{array}{l} \langle \rho(\phi)\mathbf{u}_t, \bar{\mathbf{u}} \rangle + ([(\rho(\phi)\mathbf{u} - \rho_{diff}m(\phi)\nabla w) \cdot \nabla]\mathbf{u}, \bar{\mathbf{u}}) \\ \quad + 2(\eta(\phi)\mathbf{D}\mathbf{u}, \mathbf{D}\bar{\mathbf{u}}) - (p, \nabla \cdot \bar{\mathbf{u}}) + (\phi\nabla w, \bar{\mathbf{u}}) = 0, \\ (\nabla \cdot \mathbf{u}, \bar{p}) = 0, \\ \langle \phi_t, \bar{w} \rangle - (\mathbf{u} \phi, \nabla\bar{w}) + (m(\phi)\nabla w, \nabla\bar{w}) = 0, \\ \lambda\varepsilon(\nabla\phi, \nabla\bar{\phi}) + \frac{\lambda}{\varepsilon}(f(\phi), \bar{\phi}) - (w, \bar{\phi}) = 0. \end{array} \right. \tag{2.6}$$

Taking $\bar{w} = 1$ as test function in (2.6)₃, one deduces directly the conservation property (standard for Cahn-Hilliard models):

$$\frac{d}{dt} \int_{\Omega} \phi(t, x) dx = 0. \tag{2.7}$$

On the other hand, taking as test functions $\bar{\mathbf{u}} = \mathbf{u}$, $\bar{p} = p$, $\bar{w} = w$ and $\bar{\phi} = \phi_t$ in (2.6), and testing the ρ -equation (2.1)₃ by $|\mathbf{u}|^2/2$, the following (dissipative) energy law holds:

$$\frac{d}{dt} \int_{\Omega} \left(\rho(\phi) \frac{|\mathbf{u}|^2}{2} + \frac{\lambda\varepsilon}{2} |\nabla\phi|^2 + \frac{\lambda}{\varepsilon} F(\phi) \right) dx + 2 \int_{\Omega} \eta(\phi) |\mathbf{D}\mathbf{u}|^2 dx + \int_{\Omega} m(\phi) |\nabla w|^2 dx = 0. \tag{2.8}$$

In particular, this energy law implies the dissipative character of the free energy

$$E(\mathbf{u}, \phi) = \int_{\Omega} \rho(\phi) \frac{|\mathbf{u}|^2}{2} + \frac{\lambda\varepsilon}{2} \int_{\Omega} |\nabla\phi|^2 + \frac{\lambda}{\varepsilon} \int_{\Omega} F(\phi) dx,$$

which is sum of the kinetic energy, the philic energy and the phobic one, respectively.

3. Numerical Schemes

Our aim is to design numerical schemes to approximate model (2.6) by Finite Elements in space and Finite Differences in time, satisfying a discrete version of the energy law (2.8) (in Definition 3.1 we introduce the concept of energy-stable schemes). Furthermore, we present a linear splitting algorithm that decouples the computation of the fluid part from the phase-field one maintaining the energy stability. For simplicity, we assume the uniform partition of the time interval: $t^n = nk$, with a fixed time step $k > 0$. Hereafter, we denote

$$\delta_t a^{n+1} = \frac{a^{n+1} - a^n}{k}.$$

Definition 3.1. A numerical scheme is energy-stable if it holds

$$\delta_t E(\mathbf{u}^{n+1}, \phi^{n+1}) + 2 \int_{\Omega} \eta(\phi^n) |\mathbf{D}\mathbf{u}^{n+1}|^2 dx + \int_{\Omega} m(\phi^n) |\nabla w^{n+1}|^2 dx \leq 0, \quad \forall n.$$

In particular, energy-stable schemes satisfy the energy decreasing in time property,

$$E(\mathbf{u}^{n+1}, \phi^{n+1}) \leq E(\mathbf{u}^n, \phi^n), \quad \forall n.$$

Remark 3.1. To define our scheme, a few remarks are in order:

1. In order to get the energy-stability of the scheme, it is necessary to maintain the energy law (2.8) at discrete level.
2. Once this discrete energy law holds, it is important to maintain the positivity of $\rho(\phi)$, $\eta(\phi)$ and $m(\phi)$, in order to deduce the dissipation of the scheme (as in the continuous problem).
3. A scheme splitting the Cahn-Hilliard unknowns (ϕ, w) from the Navier-Stokes one (\mathbf{u}, p) is desirable to save computational cost.

3.1. Description of the scheme

Taking into account Remark 3.1, we have designed the following scheme:

Let $(\mathbf{u}^n, p^n, \phi^n, w^n) \in \mathbf{V} \times P \times X \times W \subset (\mathbf{H}_0^1(\Omega), L_0^2(\Omega), H^1(\Omega), H^1(\Omega))$ be known (in practice, \mathbf{V}, P, X, W will be a Finite Element spaces, related to a regular triangulation of Ω).

- **Step 1:** Compute the following truncation of ϕ^n :

$$[\phi^n] = \begin{cases} -1 & \text{if } \phi^n(x) < -1, \\ \phi^n(x) & \text{if } \phi^n(x) \in [-1, 1], \\ 1 & \text{if } \phi^n(x) > 1. \end{cases}$$

and the modified density

$$\rho([\phi^n]) = \frac{\rho_1 + \rho_2}{2} + \frac{\rho_1 - \rho_2}{2} [\phi^n] = \rho_{med} + \rho_{dif} [\phi^n] \tag{3.1}$$

In the case of Finite-Element approximation, this truncation $[\phi^n]$ can be taken by nodes.

- **Step 2:** Find $(\phi^{n+1}, w^{n+1}) \in X \times W$ such that, for each $(\bar{\phi}, \bar{w}) \in X \times W$,

$$\begin{cases} \left(\frac{\phi^{n+1} - \phi^n}{k}, \bar{w} \right) - ([\phi^n] \mathbf{u}^*, \nabla \bar{w}) + (m([\phi^n]) \nabla w^{n+1}, \nabla \bar{w}) = 0 \\ \lambda \varepsilon (\nabla \phi^{n+1}, \nabla \bar{\phi}) + \frac{\lambda}{\varepsilon} (f_k(\phi^{n+1}, \phi^n), \bar{\phi}) = (w^{n+1}, \bar{\phi}) \end{cases} \tag{3.2}$$

where

$$\mathbf{u}^* = \mathbf{u}^n - k \frac{[\phi^n]}{\rho([\phi^n])} \nabla w^{n+1} \tag{3.3}$$

and $f_k(\phi^{n+1}, \phi^n)$ denotes any first-order approximation of $f(\phi(t_{n+1}))$.

• **Step 3:** Find $(\mathbf{u}^{n+1}, p^{n+1}) \in \mathbf{V} \times P$ such that, for each $(\bar{\mathbf{u}}, \bar{p}) \in V \times P$,

$$\left\{ \begin{array}{l} \left(\rho([\phi^n]) \frac{\mathbf{u}^{n+1} - \mathbf{u}^n}{k}, \bar{\mathbf{u}} \right) + \frac{1}{2} \left(\mathbf{u}^{n+1} \frac{\rho([\phi^{n+1}]) - \rho([\phi^n])}{k}, \bar{\mathbf{u}} \right) \\ + c \left(\rho(\phi^n) \mathbf{u}^n - \rho_{dif} m(\phi^n) \nabla w^{n+1}, \mathbf{u}^{n+1}, \bar{\mathbf{u}} \right) \\ + \left(2\eta([\phi^n]) \mathbf{D}\mathbf{u}^{n+1}, \mathbf{D}\bar{\mathbf{u}} \right) - \left(p^{n+1}, \nabla \cdot \bar{\mathbf{u}} \right) = - \left([\phi^n] \nabla w^{n+1}, \bar{\mathbf{u}} \right), \\ \left(\nabla \cdot \mathbf{u}^{n+1}, \bar{p} \right) = 0, \end{array} \right. \quad (3.4)$$

where

$$c(\mathbf{u}, \mathbf{v}, \mathbf{w}) := \left((\mathbf{u} \cdot \nabla) \mathbf{v}, \mathbf{w} \right) + \frac{1}{2} \left(\nabla \cdot \mathbf{u}, \mathbf{v} \cdot \mathbf{w} \right)$$

and $\rho([\phi^{n+1}])$ is computed as in (3.1).

Remark 3.2. It suffices to take $\bar{\phi} = 1$ in (3.2) to deduce the discrete in time version of the conservative property (2.7):

$$\int_{\Omega} \phi^{n+1} dx = \int_{\Omega} \phi^n dx.$$

This equality is also valid when a Finite-Element spatial approximation is considered.

Remark 3.3. From (3.3), one has

$$\rho([\phi^n]) \frac{\mathbf{u}^{n+1} - \mathbf{u}^n}{k} + [\phi^n] \nabla w^{n+1} = \rho([\phi^n]) \frac{\mathbf{u}^{n+1} - \mathbf{u}^*}{k}, \quad (3.5)$$

hence (3.4) can be rewritten as

$$\left\{ \begin{array}{l} \left(\rho([\phi^n]) \frac{\mathbf{u}^{n+1} - \mathbf{u}^*}{k}, \bar{\mathbf{u}} \right) + \frac{1}{2} \left(\mathbf{u}^{n+1} \frac{\rho([\phi^{n+1}]) - \rho([\phi^n])}{k}, \bar{\mathbf{u}} \right) \\ + c \left(\rho(\phi^n) \mathbf{u}^n - \rho_{dif} m(\phi^n) \nabla w^n, \mathbf{u}^{n+1}, \bar{\mathbf{u}} \right) \\ + \left(2\eta([\phi^n]) \mathbf{D}\mathbf{u}^{n+1}, \mathbf{D}\bar{\mathbf{u}} \right) - \left(p^{n+1}, \nabla \cdot \bar{\mathbf{u}} \right) = 0, \\ \left(\nabla \cdot \mathbf{u}^{n+1}, \bar{p} \right) = 0. \end{array} \right. \quad (3.6)$$

This formulation will be appropriate to deduce energy-stability of the scheme. This idea has been used in [22] for a triphasic NSCH problem.

Remark 3.4. Starting from (2.6)₁, we arrive at (3.4) by introducing the following residual expression related to (2.6)₃:

$$\frac{1}{2} \int_{\Omega} \left(\delta_t \rho([\phi^{n+1}]) + \operatorname{div}(\rho(\phi^n) \mathbf{u}^n - \rho_{dif} m(\phi^n) \nabla w^n) \right) \mathbf{u}^{n+1} \cdot \bar{\mathbf{u}} dx.$$

This idea has been used in [14, 15] to define a stable approximation of the density-dependent Navier-Stokes problem.

3.2. Long-time stability of the scheme

Theorem 3.1. *The splitting scheme (3.2)-(3.4) is energy-stable and satisfies the following discrete energy law:*

$$\begin{aligned} \delta_t E(\mathbf{u}^{n+1}, \phi^{n+1}) + \|\sqrt{2\eta([\phi^n])} \mathbf{D}\mathbf{u}^{n+1}\|_{L^2}^2 + \|\sqrt{m([\phi^n])} \nabla w^{n+1}\|_{L^2}^2 \\ + ND_{philic}^{n+1} + ND_{phobic}^{n+1} = 0 \end{aligned} \tag{3.7}$$

where the total energy is

$$E(\mathbf{u}, \phi) = \int_{\Omega} \left(\rho([\phi]) \frac{|\mathbf{u}|^2}{2} + \frac{\lambda\varepsilon}{2} |\nabla \phi|^2 + \frac{\lambda}{\varepsilon} F(\phi) \right) dx,$$

the philic numerical dissipation is

$$ND_{philic}^{n+1} = k \frac{\lambda\varepsilon}{2} \|\delta_t \nabla \phi^{n+1}\|_{L^2}^2 + \frac{k}{2} \int_{\Omega} \rho([\phi^n]) \left(\left| \frac{\mathbf{u}^n - \mathbf{u}^*}{k} \right|^2 + \left| \frac{\mathbf{u}^* - \mathbf{u}^{n+1}}{k} \right|^2 \right) dx$$

and the phobic numerical dissipation (or source) is

$$ND_{phobic}^{n+1} = \frac{\lambda}{\varepsilon} \int_{\Omega} f_k(\phi^{n+1}, \phi^n) \delta_t \phi^{n+1} dx - \frac{\lambda}{\varepsilon} \delta_t \int_{\Omega} F(\phi^{n+1}) dx.$$

Proof. Taking $(\bar{w}, \bar{\phi}) = (w^{n+1}, \delta_t \phi^{n+1})$ in (3.2), we obtain

$$\begin{aligned} -\left(\mathbf{u}^* [\phi^n], \nabla w^{n+1} \right) + \|\sqrt{m([\phi^n])} \nabla w^{n+1}\|_{L^2}^2 + \frac{\lambda}{\varepsilon} \delta_t \int_{\Omega} F(\phi^{n+1}) dx \\ + \frac{\lambda\varepsilon}{2} \delta_t \|\nabla \phi^{n+1}\|_{L^2}^2 + k \frac{\lambda\varepsilon}{2} \|\delta_t \nabla \phi^{n+1}\|_{L^2}^2 + ND_{phobic}^{n+1} = 0. \end{aligned} \tag{3.8}$$

Taking $(\bar{\mathbf{u}}, \bar{p}) = (\mathbf{u}^{n+1}, p^{n+1})$ in (3.6), we obtain

$$\begin{aligned} \frac{1}{2} \int_{\Omega} \rho([\phi^n]) \frac{|\mathbf{u}^{n+1}|^2 - |\mathbf{u}^*|^2 + |\mathbf{u}^{n+1} - \mathbf{u}^*|^2}{k} dx + \frac{1}{2} \int_{\Omega} \frac{\rho([\phi^{n+1}]) - \rho([\phi^n])}{k} |\mathbf{u}^{n+1}|^2 dx \\ + \|\sqrt{2\eta([\phi^n])} \mathbf{D}\mathbf{u}^{n+1}\|_{L^2}^2 = 0, \end{aligned}$$

hence

$$\begin{aligned} \frac{1}{2k} \int_{\Omega} \rho([\phi^{n+1}]) |\mathbf{u}^{n+1}|^2 - \frac{1}{2k} \int_{\Omega} \rho([\phi^n]) |\mathbf{u}^*|^2 + \frac{k}{2} \int_{\Omega} \rho([\phi^n]) \left| \frac{\mathbf{u}^* - \mathbf{u}^{n+1}}{k} \right|^2 dx \\ + \|\sqrt{2\eta([\phi^n])} \mathbf{D}\mathbf{u}^{n+1}\|_{L^2}^2 = 0. \end{aligned} \tag{3.9}$$

On the other hand, rewritten (3.3) as

$$\rho([\phi^n]) \frac{\mathbf{u}^* - \mathbf{u}^n}{k} + [\phi^n] \nabla w^{n+1} = 0$$

and testing by \mathbf{u}^* ,

$$\frac{1}{2} \int_{\Omega} \rho([\phi^n]) \frac{|\mathbf{u}^*|^2 - |\mathbf{u}^n|^2 + |\mathbf{u}^n - \mathbf{u}^*|^2}{k} dx + \left([\phi^n] \nabla w^{n+1}, \mathbf{u}^* \right) = 0. \tag{3.10}$$

Finally, adding relations (3.8)-(3.10), the first term of (3.8) cancels with the last term of (3.10), hence (3.7) holds. □

Remark 3.5. Since the philic numerical dissipation ND_{philic}^{n+1} is positive, the linearity and the unconditional energy-stability of scheme (3.2)-(3.4) will depend on the approximation considered $f_k(\phi^{n+1}, \phi^n)$ for the potential term $f(\phi(t_{n+1}))$, which gives the expression of the phobic numerical dissipation/source ND_{phobic}^{n+1} . For a detailed study of different ways of defining $f_k(\phi^{n+1}, \phi^n)$ (and the related ND_{phobic}^{n+1} to each case) for Allen-Cahn and Cahn-Hilliard models, we refer the reader to [16, 17] and the references therein.

Remark 3.6. Convergence results as $k, h \rightarrow 0$ towards weak solutions of problem (2.3) remains as an open problem. In fact, even assuming some type of convergence, it will arrive at a limit system like (2.6) but with a truncated density. Since problem (2.6) has not a maximum principle for the density yielding to $-1 \leq \rho(t, x) \leq 1$ a.e. $(t, x) \in Q$, then it is not clear if systems (2.6) with and without truncation for the density are equivalent problems.

4. Numerical Simulations

To show the effectiveness of the numerical scheme (3.2)-(3.4) in different situations, in this section we present some numerical simulations that we have carried out using **FreeFem++** software [11].

In each case we show the time dynamic of the phase and the velocity. Moreover, at the end of each experiment, the time dynamic of kinetic energy, mixing energy (sum of the philic and phobic one) and the equilibrium criterium $\|w^{n+1}\|_{L^2(\Omega)}^2$ (which tends to zero in the equilibrium states) are presented.

In all cases, we are introducing the gravity as an external force in the \mathbf{u} -system (2.1)₁, so we can not expect a strictly decreasing energy property. In fact, a force term $-\rho \mathbf{g}$ is introduced at the LHS of (2.1)₁, where $\mathbf{g} = (0, g)^t$ with $g > 0$ being the (constant) gravity acceleration. Notice that this term cannot be treated as a gradient term because the density ρ is variable.

We consider the following values for the parameters, while λ , the initial data and the densities

Table 4.1: Parameters

ε	h	dt	$\eta(\phi)$	$m(\phi)$
10^{-2}	$1/90$	10^{-2}	1	1

ρ_1, ρ_2 will be detailed in each case.

The potential approximation considered for the numerical simulations is the linear second order in time approximation introduced in [16] (and also studied in [17]):

$$f_k(\phi^{n+1}, \phi^n) := f(\phi^n) + \frac{1}{2}f'(\phi^n)(\phi^{n+1} - \phi^n) = \frac{3}{2}(\phi^n)^2\phi^{n+1} - \frac{1}{2}(\phi^n)^3 - \frac{\phi^{n+1} + \phi^n}{2}. \quad (4.1)$$

It is known that for a regular enough exact solution $\phi(t)$, this approximation has second order accuracy with respect to $f(\phi(t))$ and it also introduces second order phobic numerical dissipation (this fact is very important to assure that the scheme is not introducing too much dissipation in the discrete energy law (3.7)):

$$\|f(\phi(t_{n+1})) - f_k(\phi(t_{n+1}), \phi(t_n))\|_{L^2(\Omega)} = O(k^2) \quad \text{and} \quad ND_{phobic}(\phi(t_{n+1}), \phi(t_n)) = O(k^2).$$

We choose the Mini Element Finite-Element approximation for the fluid part and P_1 Finite Element approximation for each phase unknown, i.e.,

$$(\mathbf{V}, P) \sim P_1 - \text{bubble}/P_1, \quad (X, W) \sim P_1 \times P_1.$$

See Appendix for the well-posedness of the corresponding fully discrete scheme.

We present three types of numerical simulations:

1. A heavier bubble falling in a lighter medium in 2D.

As in [23], we consider the situation where a bubble with density ρ_1 initially inside a medium with lower density ρ_2 confined in the square domain $\Omega = [0, 1] \times [0, 1]$. In this case, we see how the heavier bubble falls to the bottom of the domain. Firstly we consider $(\rho_1, \rho_2) = (100, 1)$ and secondly $(\rho_1, \rho_2) = (1000, 1)$.

In this case, the fluid with density ρ_2 is represented using red color (or clear color) meanwhile blue color (or dark color) has been chosen to plot the ρ_1 case. We can observe how the heavier fluid falls more quickly in the case of more difference between the densities.

2. Rayleigh-Taylor instability in 2D.

Inspired in the simulations presented in [5, 13] (and the references therein), we consider as initial condition a heavier fluid on the top with density ρ_1 (and a lighter fluid on the bottom with density ρ_2) in the domain $\Omega = [0, 1] \times [0, 1]$ and we see how the lighter fluid rises until it arrives at the equilibrium with the lighter fluid in the top (and the heavier in the bottom). Firstly we consider $(\rho_1, \rho_2) = (100, 1)$ and secondly $(\rho_1, \rho_2) = (1000, 1)$.

In this case, the fluid with density ρ_1 is represented using red color (or clear color) meanwhile blue color (or dark color) has been chosen to plot the ρ_2 case.

Furthermore, in both 2D simulations we also study the influence of the parameter λ in the system. In each simulation, every figure represent one instant of time with three columns in order to show the differences of the behavior with respect to the choice of λ . In particular, the left column corresponds to $\lambda = 10^{-2}$, the centre one to $\lambda = 10^{-3}$ and the right column represents the case of $\lambda = 10^{-4}$. We can observe how the rigidity of the interface increases as λ increases and how the conservation of volume is achieved in all cases.

3. 3D Numerical simulations.

In order to show the efficiency of the numerical scheme we extend the simulations presented in the previous subsections to the 3D case. We consider the domain $\Omega = [0, 1] \times [0, 1] \times [0, 1]$ and we see how the heavier fluid falls until it arrives at the equilibrium with the lighter fluid in the top (and the heavier in the bottom). In this case, we consider the following values for the parameters

Table 4.2: Parameters

ε	h	dt	$\eta(\phi)$	$m(\phi)$	ρ_1	ρ_2
10^{-2}	1/30	10^{-2}	1	1	100	1

4.1. First experiment: a heavier bubble falling in a lighter medium

In subsections 4.1.1 and 4.1.2 we see how the bubble falls until they broke and arrives to a equilibrium state where the heavier fluid fills the bottom of the domain. In both cases, we can observe the differences in the behaviors with respect to the choice of λ . Indeed, the lower the value of parameter λ is, the higher the influence of the fluid in the system, as can be appreciated in the evolution of the dynamics (Figs. 4.1 and 4.3) and in the energy plots in Figs. 4.2 and 4.4. The equilibrium ($\|w^{n+1}\|_{L^2(\Omega)}$) tends to zero when the system is arriving to the equilibrium solution (Figs. 4.2 and 4.4).

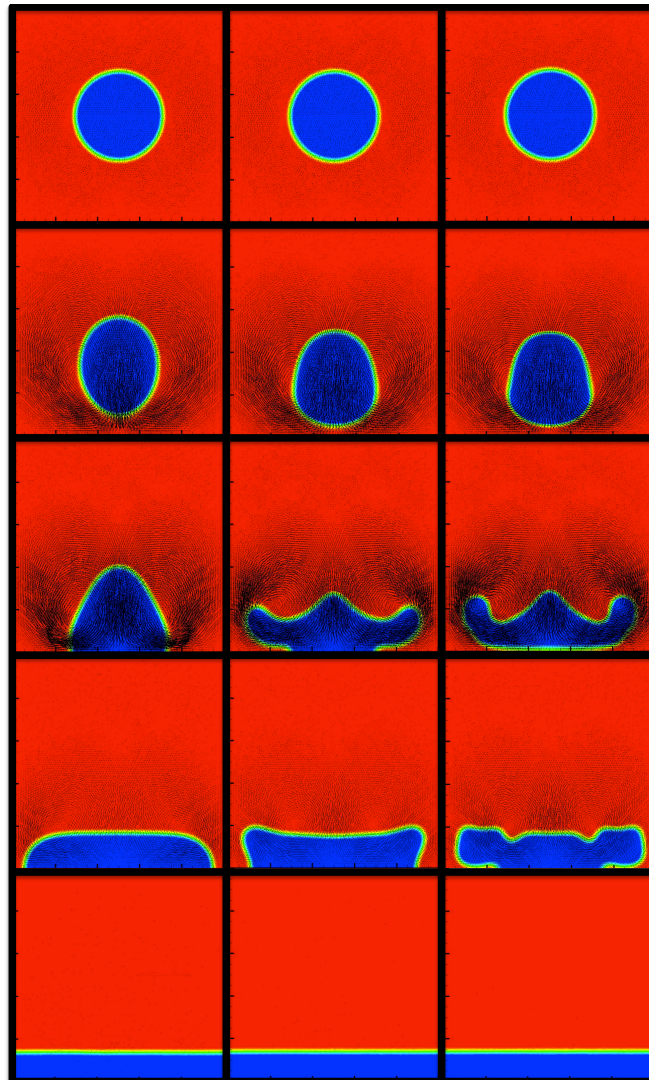


Fig. 4.1. Left $\lambda = 10^{-2}$, centre $\lambda = 10^{-3}$ and right $\lambda = 10^{-4}$ ($\rho_1 = 100, \rho_2 = 1$). Time=0.01, 0.3, 0.5, 1.0 and 10.0 .

4.1.1. A heavier bubble falling in a lighter medium. $\rho_1 = 100, \rho_2 = 1$

The evolution of the energies (kinetic and mixing) and equilibrium are presented in Fig. 4.2.

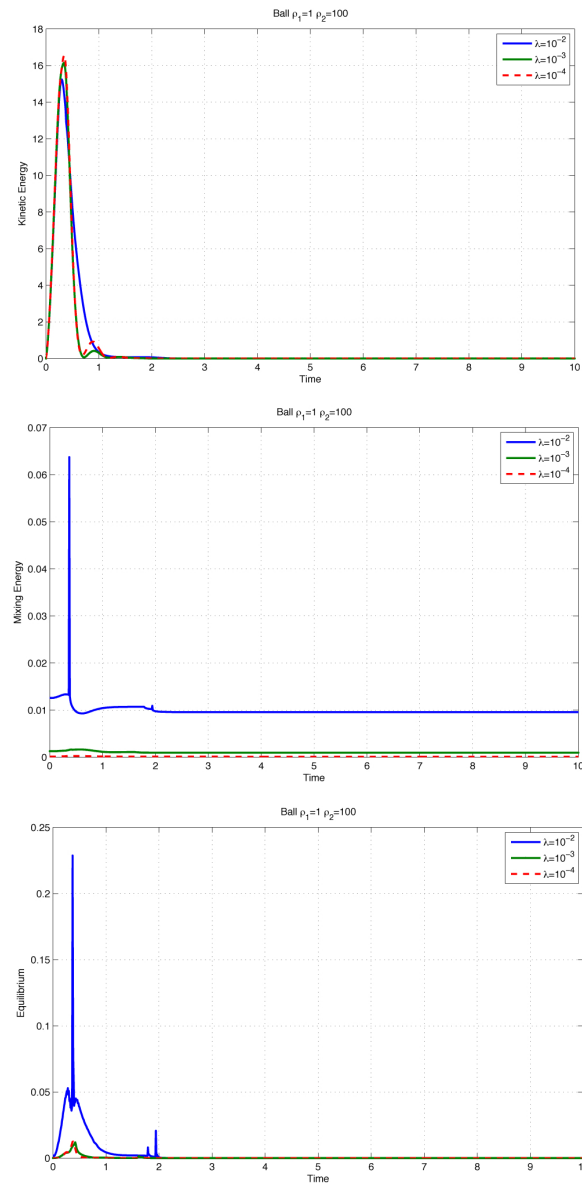


Fig. 4.2. Kinetic Energy, Mixing Energy and Equilibrium in $[0, 10]$.

4.1.2. A heavier bubble falling in a lighter medium. $\rho_1 = 1000, \rho_2 = 1$

The evolution of the energies (kinetic and mixing) and equilibrium are presented in Fig. 4.4.

4.2. Second experiment: Rayleigh-Taylor instability

In this experiment we present the evolution of two fluids with different densities when the heavier fluid is on the top of the domain and the interface between them is a small perturbation from a straight line. We see how the fluids evolves in time, considering two different density ratios and with different choices of the parameter λ . As in the previous experiment, it can be

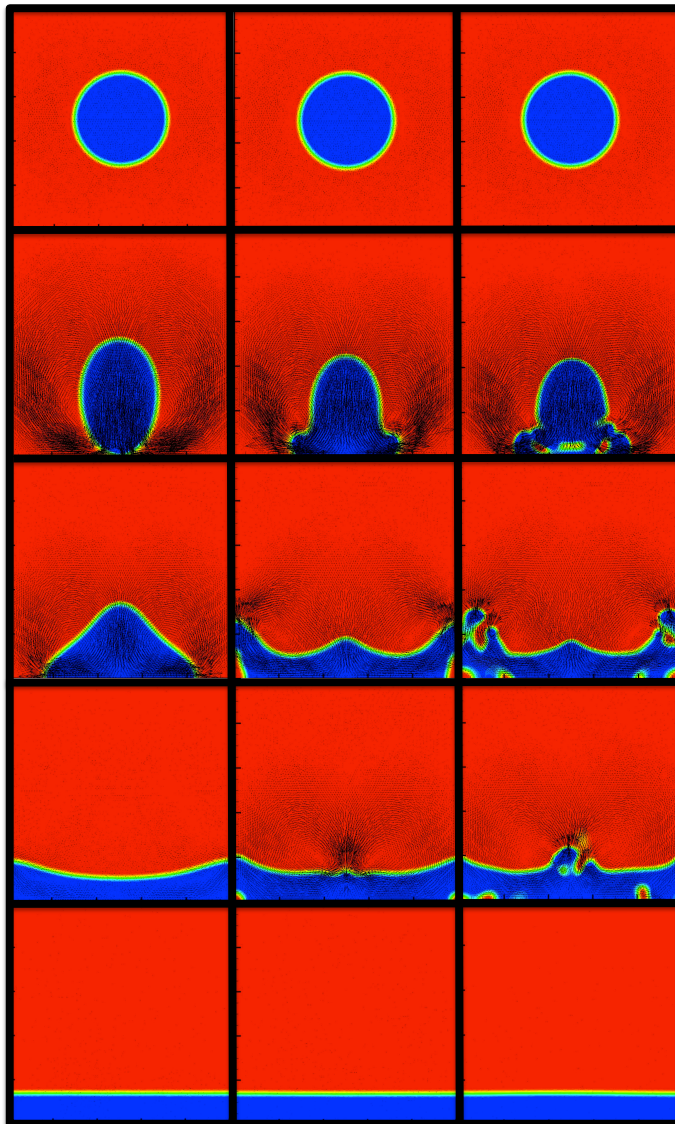


Fig. 4.3. Left $\lambda = 10^{-2}$, centre $\lambda = 10^{-3}$ and right $\lambda = 10^{-4}$ ($\rho_1 = 1000, \rho_2 = 1$). Time=0.01, 0.3, 1.0 and 10.0 .

observed the influence of the parameter λ in the evolution of the dynamics (Figs. 4.5 and 4.7) and in the energy plots in Figs. 4.6 and 4.8. Furthermore, in Figs. 4.6 and 4.8 it is shown how the equilibrium ($\|w^{n+1}\|_{L^2(\Omega)}^2$) tends to zero when the system is arriving to the equilibrium solution is presented.

4.2.1. Rayleigh-Taylor instability. $\rho_1 = 100, \rho_2 = 1$

The evolution of the energies (kinetic and mixing) and equilibrium are presented in Fig. 4.6.

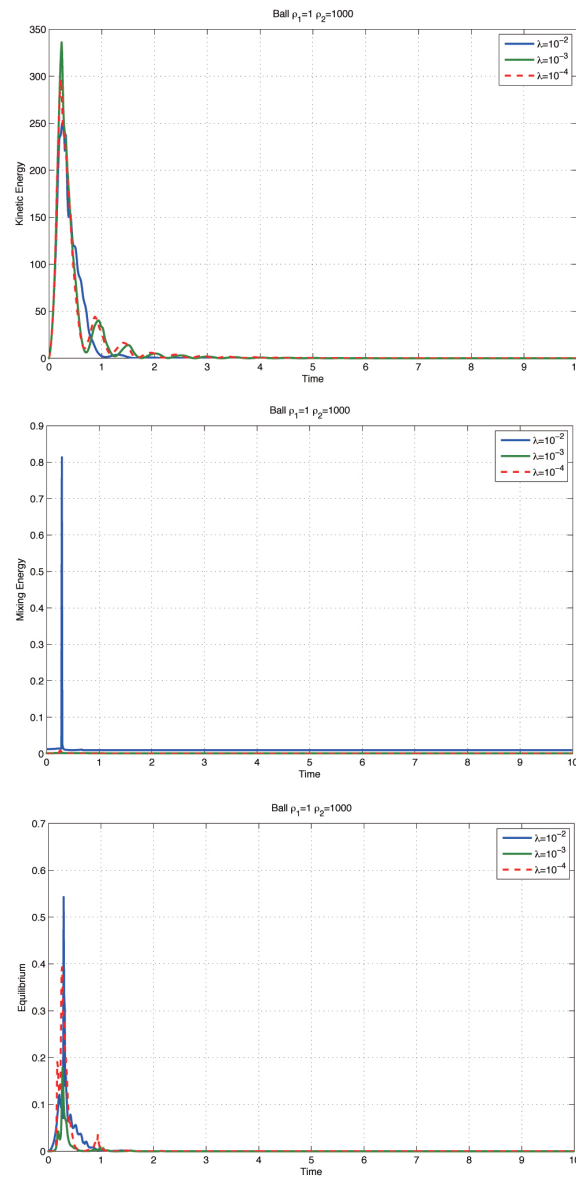


Fig. 4.4. Kinetic Energy, Mixing Energy and Equilibrium in $[0, 10]$.

4.2.2. Rayleigh-Taylor instability. $\rho_1 = 1000$, $\rho_2 = 1$

The evolution of the energies (kinetic and mixing) and equilibrium are presented in Fig. 4.8.

4.3. 3D Simulations

In Figs. 4.9 and 4.10 we show the extension of the previous simulations to the 3D case. We observe how in both cases the heavier fluid falls until they arrive to a equilibrium state filling the bottom of the domain. The results obtained in these subsections show the validity of these kind of schemes to carry out 3D simulations.

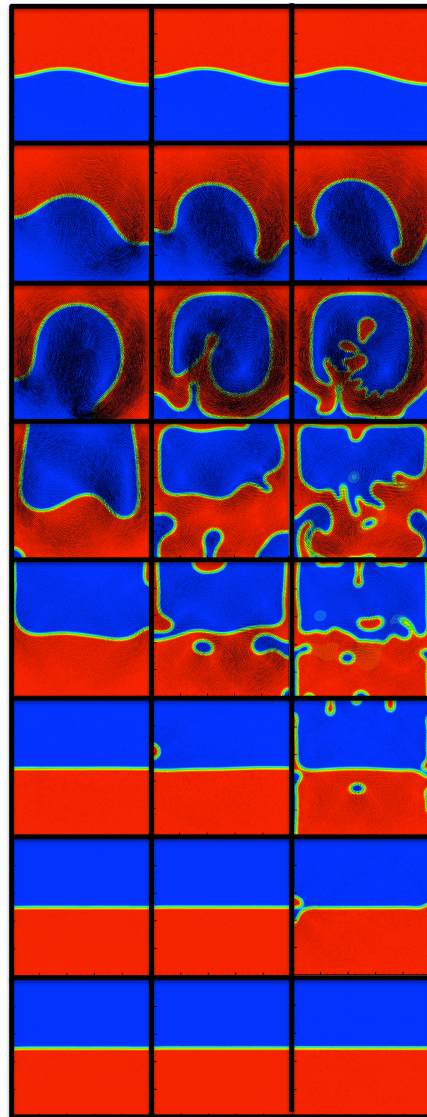


Fig. 4.5. Left $\lambda = 10^{-2}$, centre $\lambda = 10^{-3}$ and right $\lambda = 10^{-4}$ ($\rho_1 = 100, \rho_2 = 1$). Time=0.01, 0.5, 1.0, 2.0, 3.0, 5.0, 8.0 and 10.0 .

4.3.1. A heavier bubble falling in a lighter medium. $\rho_1 = 100, \rho_2 = 1, \lambda = 0.0005$

4.3.2. Rayleigh-Taylor instability. $\rho_1 = 100, \rho_2 = 1, \lambda = 0.01$

5. Conclusions

We claim that the results presented in this paper contributes to confirm (from the numerical point of view) the validity of the model proposed by Abels et al. in [3].

In this paper, we have presented a new numerical scheme to approximate a thermodynamically consistent model recently introduced in the literature to represent the behavior of two immiscible and incompressible fluids with different densities. The main advantage of this scheme

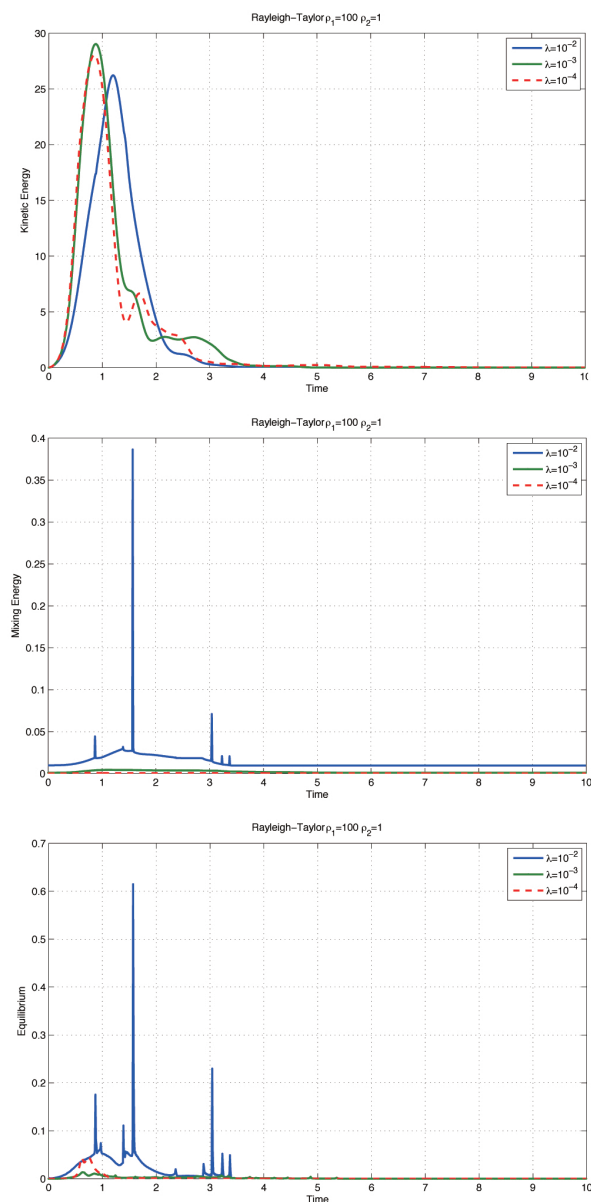


Fig. 4.6. Kinetic Energy, Mixing Energy and Equilibrium in $[0, 10]$.

is that it splits the problem between fluid part and phase-field part in a linear way, reducing the computational complexity of the scheme (compared with the fully coupled one). Furthermore, we prove that this splitting scheme is energy-stable, i.e., it satisfies a discrete version of the original energy law and it is also shown that the long-time stability of the scheme will depend on the choice of the double-well (polynomial) potential approximation considered.

We report the result of several numerical simulations. From these results, we have observed the efficiency in time of the proposed algorithm. The scheme allows us to compare different situations under a reasonable computational cost, studying the influence of the choice of the densities and the surface tension parameter and we have also been able to compute some $3D$

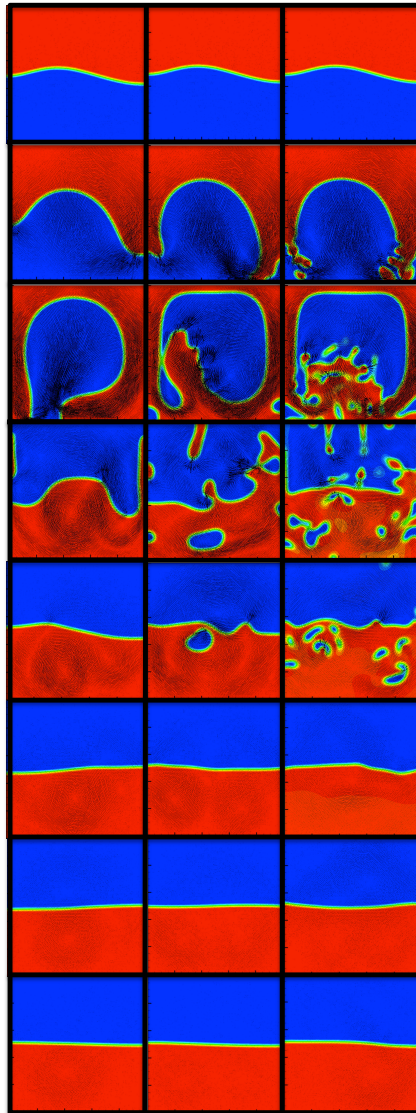


Fig. 4.7. Left $\lambda = 10^{-2}$, centre $\lambda = 10^{-3}$ and right $\lambda = 10^{-4}$ ($\rho_1 = 1000, \rho_2 = 1$). Time=0.01, 0.5, 1.0, 2.0, 3.0, 5.0, 8.0 and 10.0 .

numerical experiments, to demonstrate the applicability of this scheme to more realistic physical problems. Indeed, it is shown how this scheme capture rather well complicated dynamics like the Rayleigh-Taylor instability.

A. Appendix: Well-posedness of the fully discrete scheme

In this appendix, we study the existence and uniqueness of the systems (3.2) and (3.4), considering the finite element approximation in space used in the numerical simulations, that is $(\mathbf{V}_h, P_h) \sim P_1 - bubble/P_1$ and $(X_h, W_h) \sim P_1 \times P_1$.

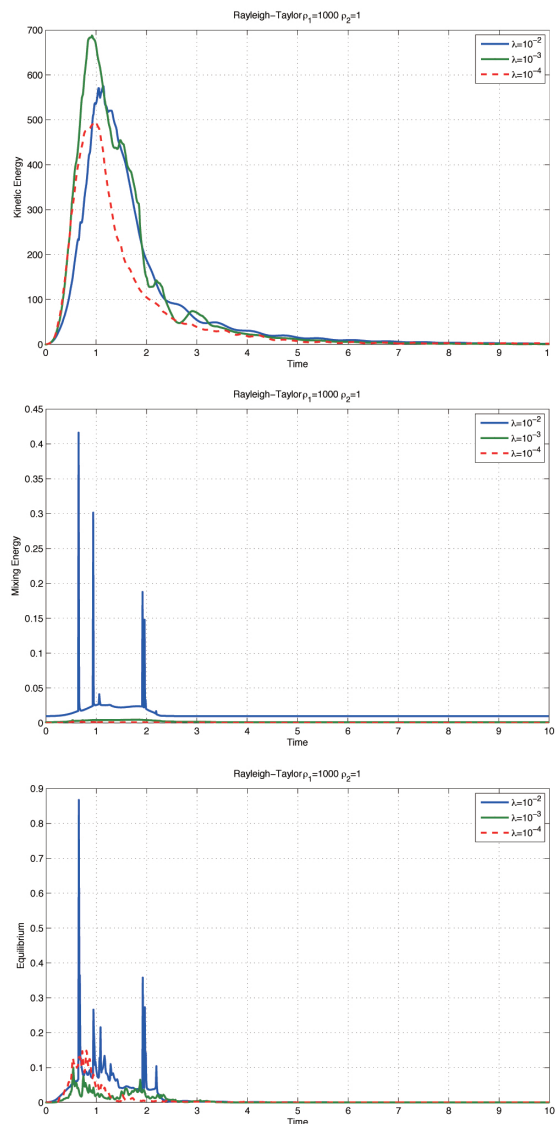


Fig. 4.8. Kinetic Energy, Mixing Energy and Equilibrium in $[0, 10]$.

The study of problem (3.2) depends on the choice of the potential term. In particular, we focus on the approximation (4.1) considered in the numerical simulations.

Lemma A.1. *There exists an unique solution of (3.2) with the potential approximation (4.1), under the constraint $k < 8\epsilon^3/(\lambda \widehat{m}([\phi^n]))$, where*

$$\widehat{m}([\phi^n]) = m([\phi^n]) + k \frac{[\phi^n]^2}{\rho([\phi^n])}.$$

Proof. Since (3.2) (taking (4.1)) is an algebraic square linear system, it suffices to prove uniqueness. Indeed, let $(\phi_1^{n+1}, w_1^{n+1})$ and $(\phi_2^{n+1}, w_2^{n+1})$ be two possible solutions and denoting

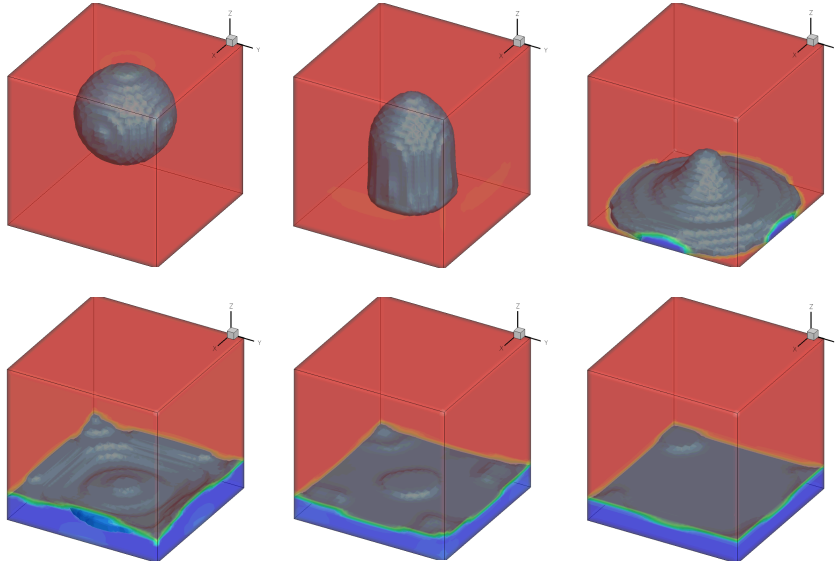


Fig. 4.9. A heavier bubble falling in a lighter medium with $\lambda = 0.0005$. Time= 0.01, 3.0, 6.0, 9.0, 14.0 and 25.0.

$\phi = \phi_1^{n+1} - \phi_2^{n+1}$ and $w = w_1^{n+1} - w_2^{n+1}$, we arrive at

$$\begin{cases} \frac{1}{k}(\phi, \bar{w}) - ([\phi^n] \mathbf{u}^*(w), \nabla \bar{w}) + (m([\phi^n]) \nabla w, \nabla \bar{w}) = 0, & \forall \bar{w} \in W_h, \\ \lambda \varepsilon (\nabla \phi, \nabla \bar{\phi}) + \frac{\lambda}{2\varepsilon} (f'(\phi^n) \phi, \bar{\phi}) = (w, \bar{\phi}), & \forall \bar{\phi} \in X_h, \end{cases} \quad (\text{A.1})$$

where

$$\mathbf{u}^*(w) = \mathbf{u}^*(w_1^{n+1}) - \mathbf{u}^*(w_2^{n+1}) = -k \frac{[\phi^n]}{\rho([\phi^n])} \nabla w.$$

The first equation of (A.1) can be rewritten as

$$\frac{1}{k}(\phi, \bar{w}) + (\hat{m}([\phi^n]) \nabla w, \nabla \bar{w}) = 0, \quad \text{with} \quad \hat{m}([\phi^n]) = m([\phi^n]) + k \frac{[\phi^n]^2}{\rho([\phi^n])}. \quad (\text{A.2})$$

Testing by $\bar{w} = w$ and $\bar{\phi} = \frac{1}{k} \phi$, we obtain

$$\int_{\Omega} \hat{m}([\phi^n]) |\nabla w|^2 + \frac{\lambda \varepsilon}{k} \|\nabla \phi\|_{L^2}^2 + \frac{\lambda}{2\varepsilon k} \int_{\Omega} f'(\phi^n) \phi^2 = 0,$$

hence, applying that $f'(\phi^n) = 3(\phi^n)^2 - 1$,

$$\int_{\Omega} \hat{m}([\phi^n]) |\nabla w|^2 + \frac{\lambda \varepsilon}{k} \|\nabla \phi\|_{L^2}^2 + \frac{\lambda}{2\varepsilon k} \int_{\Omega} 3(\phi^n)^2 \phi^2 = \frac{\lambda}{2\varepsilon k} \int_{\Omega} \phi^2. \quad (\text{A.3})$$

In order to control the right hand-side term $\frac{\lambda}{2\varepsilon k} \int_{\Omega} \phi^2$, we take $\bar{w} = \frac{\lambda}{2\varepsilon} \phi$ in (A.2) (which is

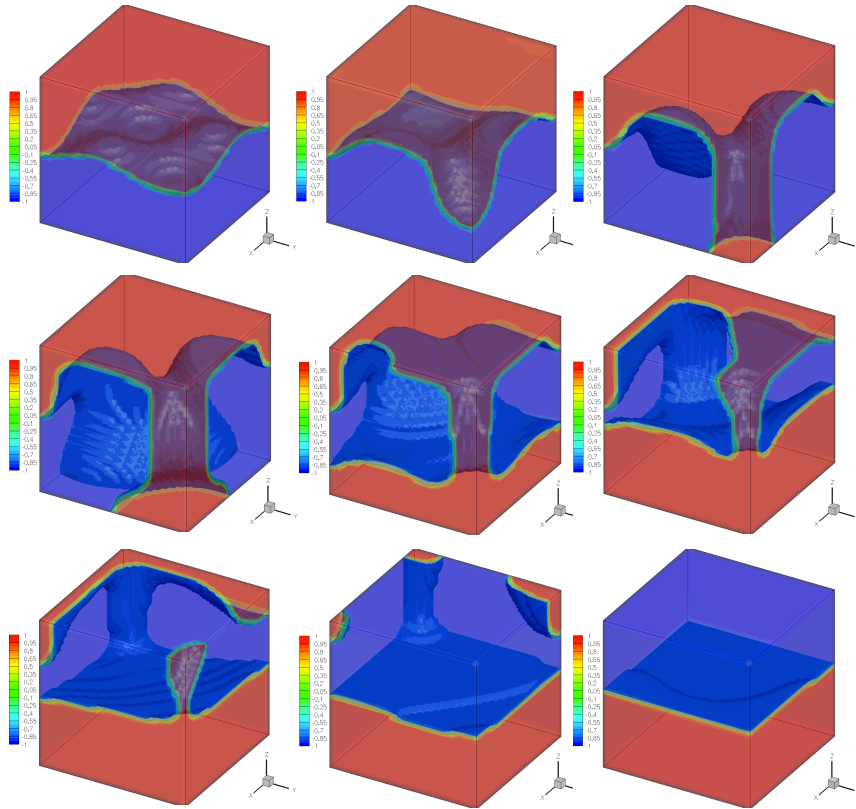


Fig. 4.10. Rayleigh-Taylor instability with $\lambda = 0.01$. Time= 0.01, 5.0, 10.0, 15.0, 18.0, 22.0, 28.0, 35.0 and 50.0.

possible because $X_h = W_h$), arriving at

$$\frac{\lambda}{2\epsilon k} \int_{\Omega} \phi^2 + \frac{\lambda}{2\epsilon} \int_{\Omega} \widehat{m}([\phi^n]) \nabla w \nabla \phi = 0,$$

hence

$$\frac{\lambda}{2\epsilon k} \int_{\Omega} \phi^2 \leq \frac{1}{2} \int_{\Omega} \widehat{m}([\phi^n]) |\nabla w|^2 + \frac{\lambda^2}{8\epsilon^2} \int_{\Omega} \widehat{m}([\phi^n]) |\nabla \phi|^2.$$

Using this bound in (A.3),

$$\frac{1}{2} \int_{\Omega} \widehat{m}([\phi^n]) |\nabla w|^2 + \lambda \int_{\Omega} \left(\frac{\epsilon}{k} - \frac{\lambda \widehat{m}([\phi^n])}{8\epsilon^2} \right) |\nabla \phi|^2 + \frac{\lambda}{2\epsilon k} \int_{\Omega} 3(\phi^n)^2 \phi^2 \leq 0.$$

Considering the constraint $k < 8\epsilon^3/(\lambda \widehat{m}([\phi^n]))$, one has that $\nabla \phi = 0$ and $\nabla w = 0$, hence ϕ and w are constant functions. Finally, since $\int_{\Omega} \phi = 0$ we derive $\phi = 0$, and combining this with (A.1)₂ we obtain $w = 0$. Therefore, the uniqueness (and existence) of solution of (3.2) (taking the potential approximation given in (4.1)) is assured. \square

Note that Lemma A.1 holds whenever the FE spaces (X_h, W_h) approximating (ϕ, w) satisfy that $X_h \subset W_h$.

Lemma A.2. *There exists an unique solution of system (3.4).*

Proof. Since again (3.4) is an algebraic square linear system, it suffices to prove uniqueness. Indeed, let $(\mathbf{u}_1^{n+1}, p_1^{n+1})$ and $(\mathbf{u}_2^{n+1}, p_2^{n+1})$ be two possible solutions of (3.2), and denoting $\mathbf{u} = \mathbf{u}_1^{n+1} - \mathbf{u}_2^{n+1}$ and $p = p_1^{n+1} - p_2^{n+1}$, we arrive at

$$\left\{ \begin{array}{l} \frac{1}{k} \left(\mathbf{u} \frac{\rho([\phi^{n+1}]) + \rho([\phi^n])}{2}, \bar{\mathbf{u}} \right) + c \left(\rho(\phi^n) \mathbf{u}^n - \rho_{diff} m(\phi^n) \nabla w^n, \mathbf{u}, \bar{\mathbf{u}} \right) \\ \quad + \left(2\eta([\phi^n]) \mathbf{D}\mathbf{u}, \mathbf{D}\bar{\mathbf{u}} \right) - \left(p, \nabla \cdot \bar{\mathbf{u}} \right) = 0, \quad \forall \bar{\mathbf{u}} \in \mathbf{V}_h, \\ \left(\nabla \cdot \mathbf{u}, \bar{p} \right) = 0, \quad \forall \bar{p} \in P_h. \end{array} \right. \quad (\text{A.4})$$

Taking $\bar{\mathbf{u}} = \mathbf{u}$ and $\bar{p} = p$, we obtain:

$$\frac{1}{k} \int_{\Omega} \frac{\rho([\phi^{n+1}]) + \rho([\phi^n])}{2} |\mathbf{u}|^2 + 2 \int_{\Omega} \eta([\phi^n]) |\mathbf{D}\mathbf{u}|^2 = 0,$$

hence $\mathbf{u} = 0$. Finally, from (A.4)₁, $(p, \nabla \cdot \bar{\mathbf{u}}) = 0$ for each $p \in P_h$, hence $p = 0$ owing to the pair of FE spaces $(\mathbf{V}_h, P_h) \sim P_1\text{-bubble}/P_1$ satisfies the stability *inf-sup* (or LBB) condition [12]:

$$\exists \beta > 0, \quad \|p\|_{L^2} \leq \beta \sup_{\bar{\mathbf{u}} \in \mathbf{V}_h \setminus \{\Theta\}} \frac{(p, \nabla \cdot \bar{\mathbf{u}})}{\|\bar{\mathbf{u}}\|_{H^1}}, \quad \forall p \in P_h.$$

Note that Lemma A.2 holds whenever the velocity-pressure FE spaces (\mathbf{V}_h, P_h) satisfy the *inf-sup* condition.

Acknowledgments. This work has been partially supported by MTM2009-12927 and MTM2012-32325 (Ministerio de Economía y Competitividad, Spain). G. Tierra has also been partially supported by NIH 1 R01 GM095959-01A1 (United States).

References

- [1] H. Abels, Strong well-posedness of a diffuse interface model for a viscous, quasi-incompressible two-phase flow, *SIAM J. Math. Anal.*, **44** (2012), 316-340.
- [2] H. Abels, D. Depner and H. Garcke, Existence of weak solutions for a diffuse interface model for two-phase flows of incompressible fluids with different densities, *J. Math. Fluid Mech.*, **15**:3 (2013), 453-480.
- [3] H. Abels, H. Garcke and G. Grün, Thermodynamically consistent, frame indifferent diffuse interface models for incompressible two-phase flows with different densities, *Math. Models Methods Appl. Sci.*, **22**:03 (2012), 1150013.
- [4] F. Boyer, A theoretical and numerical model for the study of incompressible mixture flows, *Computers & Fluids*, **31** (2002), 41-68.
- [5] R.C. Cabrales, F. Guillén-González and J.V. Gutiérrez-Santacreu, Stability and convergence for a complete model of mass diffusion, *Appl. Numer. Math.*, **61** (2011), 1161-1185.
- [6] F. Chen and J. Shen, Efficient energy stable schemes with spectral discretization in space for anisotropic Cahn-Hilliard systems, *Commun. Comput. Phys.*, **13** (2013), 1189-1208.
- [7] C. Collins, J. Shen and S.M. Wise, An efficient, energy stable scheme for the Cahn-Hilliard-Brinkman system, *Commun. Comput. Phys.*, **13** (2013), 929-957.
- [8] M.I.M. Copetti and C.M. Elliott, Numerical analysis of the Cahn-Hilliard equation with a logarithmic free energy, *Numer. Math.*, **63** (1992), 39-65.

- [9] Q. Du and R.A. Nicolaides, Numerical analysis of a continuum model of phase transition, *SIAM J. Numer. Anal.*, **28** (1991), 1310-1322.
- [10] C.M. Elliott, D.A. French and F.A. Milner, A Second Order Splitting Method for the Cahn-Hilliard Equation, *Numer. Math.*, **54** (1989), 575-590.
- [11] F. Hecht, New development in freefem++, *J. Numer. Math.*, **20**:3-4 (2012), 251-265.
- [12] V. Girault and P.A. Raviart, *Finite element methods for Navier-Stokes equations: Theory and Algorithms*, Berlin, Springer-Verlag, 1986.
- [13] J.L. Guermond and L. Quartapelle, A projection FEM for variable density incompressible flows, *J. Comput. Phys.*, **165** (2000), 167-188.
- [14] F. Guillén-González and J.V. Gutiérrez-Santacreu, Unconditional stability and convergence of fully discrete schemes for 2D viscous fluids models with mass diffusion, *Math. Comp.*, **77** (2008), 1495-1524.
- [15] F. Guillén-González and J.V. Gutiérrez-Santacreu, Conditional stability and convergence of a fully discrete scheme for three-dimensional Navier-Stokes equations with mass diffusion, *SIAM Journal Numer. Anal.*, **46** (2008), 2276-2308.
- [16] F. Guillén-González and G. Tierra, On linear schemes for a Cahn Hilliard Diffuse Interface Model, *J. Comput. Phys.*, **234** (2013), 140-171.
- [17] F. Guillén-González and G. Tierra, Second order schemes and time-step adaptivity for Allen-Cahn and Cahn-Hilliard models, *Comput. Math. Appl.* (2014). doi:10.1016/j.camwa.2014.07.014.
- [18] D. Gurtin, D. Polignone and J. Viñals, Two-phase binary fluids and immiscible fluids described by an order parameter, *Math. Models Methods Appl. Sci.*, **6** (1996), 815-831.
- [19] P.P. Hohenberg and B.I. Halperin, Theory of dynamic critical phenomena, *Rev. Mod. Phys.*, **49** (1977), 435-479.
- [20] J. Kim, Phase-field models for multi-component fluid flows, *Commun. Comput. Phys.*, **12** (2012), 613-661.
- [21] J. Lowengrub and L. Truskinovsky, Quasi-incompressible Cahn-Hilliard fluids and topological transitions, *Proc. R. Soc. Lond. A*, **454** (1998), 2617-2654.
- [22] S. Minjeaud, An unconditionally stable uncoupled scheme for a triphasic Cahn-Hilliard/Navier-Stokes model, *Num. Methods for PDE* **29**:2 (2013), 584-618.
- [23] J. Shen and X. Yang, A phase-field model and its numerical approximation for two-phase incompressible flows with different densities and viscosities, *SIAM J. Sci. Comput.*, **32** (2010), 1159-1179.
- [24] J. Shen, X. Yang and Q. Wang, Mass and volume conservation in phase field models for binary fluids, *Commun. Comput. Phys.*, **13** (2013), 1045-1065.
- [25] J.D. van der Waals, The thermodynamic theory of capillarity flow under the hypothesis of a continuous variation of density, *Verhandel. Konink. Akad. Weten. Amsterdam*, **1** (1893).
- [26] P. Yue, J.J. Feng, C. Liu and J. Shen, A diffuse-interface method for simulating two-phase flows of complex fluids, *J. Fluid Mech.*, **515** (2004), 293-317.
- [27] T. Zhang and Q. Wang, Cahn-Hilliard vs singular Cahn-Hilliard equations in phase field modeling, *Commun. Comput. Phys.*, **7** (2010), 362-382.